Team 6a: Gas Fueled RDE Scramjet

Gabriel Diez   Cameron Ellis   Alberto Marin Cebrian   Andrew McClaskey

Thomas Satterly   Drew Sherman

December 15, 2017

Contents

1 Abstract

Hypersonic vehicles demand high performance from every subsystem, with emphasis on a stable propulsion system and material capabilities. This project aims to investigate the feasibility of using a gas-fueled Rotating Detonation Engine (RDE) in a hypersonic vehicle with a cruise Mach of 6.5 at 1500 psf of dynamic pressure, launched on the GO1 platform. It was found that an ethylene fueled RDE, paired with a conical inlet and various cooling systems, is potentially capable of 107 seconds of flight, 45 second of which at cruise velocity. Most notable is a cruise Isp of 2080 seconds, which is substantially higher than conventional scramjet burners. The preliminary design shows that, while an RDE may be feasible for such a mission, extensive fundamental research is required to fully understand the operation of an RDE. A overview of the final design can be seen in Figure 1.
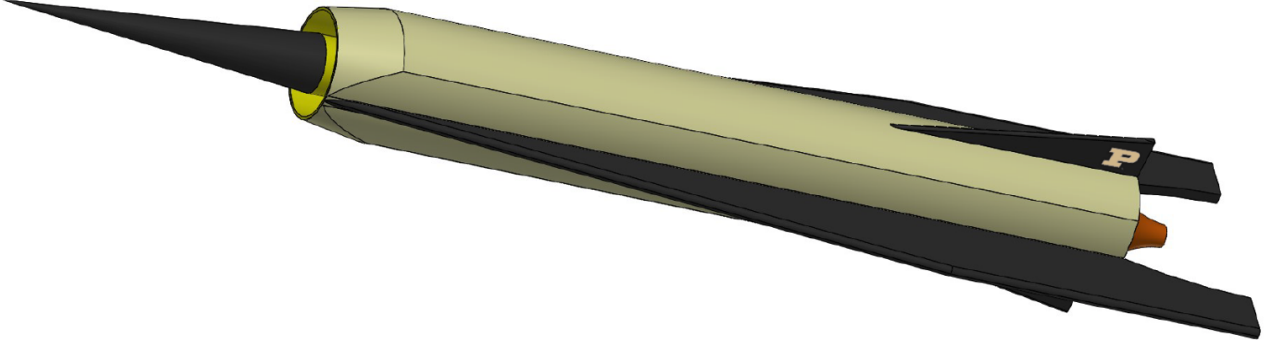
Figure 1: Overview of Final Design

2 Introduction

Sustained air-breathing hypersonic flight has been the focus of a great deal of research over the past several decades. In addition to the high temperatures associated with flight speeds higher than Mach 5, it is difficult to slow down flow speed to subsonic speeds (such as in a ramjet) for sustainable combustion without significant pressure losses, making it necessary to design combustors that can burn at supersonic velocities. One proposal for improving supersonic combustion is to modify the mechanism of reaction all together. Deflagrations require sufficient mixing of fuel and oxidizer to initiate a reaction as well as transfer energy from that reaction to the incoming flow. This is simple to accomplish at low flow speeds but deflagration proves to be an unreliable reaction mechanism at supersonic velocities. Detonations, on the other hand, are supersonic waves that flow through combustible material, reacting it as it passes [16]. Rotating Detonation Engines (RDE) have shown great promise over recent years due to their ability to maintain combustion at higher Mach numbers than traditional scramjet engines. By maintaining one or multiple detonation waves within the burner, the combustor is able to produce much higher average chamber pressures [4]. Additionally, since detonation reactions occur almost instantaneously, the combustion chamber itself can be shortened compared to traditional supersonic burners. The objective of the current work is to propose a design for a gas-injection RDE scramjet intended to be launched from a GO1 launcher to complete a cruising mission at Mach 6.5. The GO1 is capable of boosting a 600 lb vehicle to Mach 5.5 at 1500 psf of dynamic pressure [6]. The fairing requires the vehicle not exceed 24" in diameter and 120" in length.

3 Design Methodology

3.1 Vehicle Trajectory [Andy McClaskey]

The design of this vehicle was based on a 1500 pounds per square foot (71.82 kPa) constant dynamic pressure trajectory. The trajectory was found by iterating Mach number to make the density given in the dynamic pressure equation match that given by the standard atmosphere function. The altitude and velocity trajectory are shown in Appendix A in Figure 13 and Figure 14. For the specified mission of launching at Mach 5.5 and accelerating to the cruise condition at Mach 6.5 with a constant dynamic pressure of 1500 psf, the vehicle velocity varies between 1625 m/s and 1940 m/s, while the altitude varies between 23.0 km and 25.3 km.

3.2 Aerodynamic Performance Analysis [Andy McClaskey]

Aerodynamic Reference Area   The reference area needed for calculated lift and drag was determined by assuming a trapezoidal wing planform. The root and tip chord length were used as inputs to the area equation to calculate the wing planform area. The equation used for calculation total wing area is shown in Equation 1. The planform was optimized for a drag to help increase the lift to drag ratio later in the design.

$$S = (\text{Root Chord} + \text{Tip Chord}) * \frac{\text{Wing Span}}{2} \tag{1}$$

Drag Determination   The Coefficient of Drag (C_D) was taken from the 1X scale Generic Hypersonic Vehicle for the angle of attack of zero [10]. Once the coefficient of drag was known, the total drag could be calculated using Equation 2. They dynamic pressure is known from the free stream conditions of the vehicle and the aero reference area is known from above. The Coefficient of Drag is plotted in Figure 2.
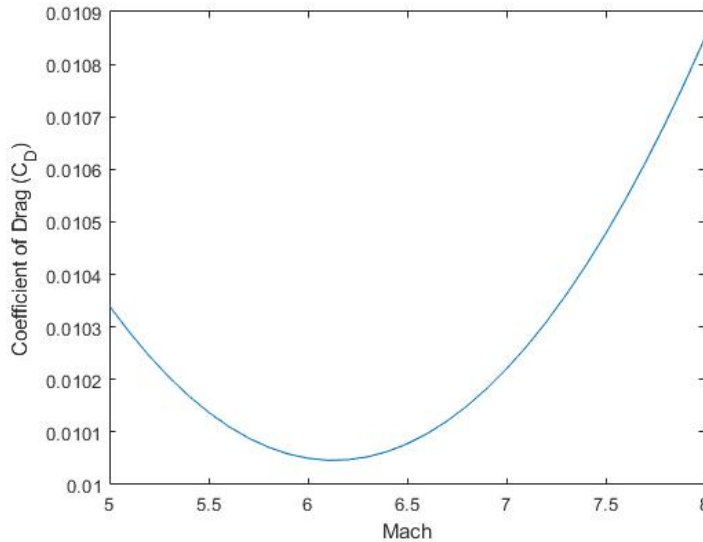
$$D = q_\infty S C_D \tag{2}$$

Figure 2: C_D v. Mach

Thrust Required   The drag determined above sets the thrust required from the propulsion system for the vehicle in straight and level unaccelerated cruise flight. For the acceleration part of the mission the thrust required is shown in Equation 3. It was assumed that the pitch angle was close to zero for this analysis.

$$\text{Thrust} = m\frac{dv}{dt} + D + mg\sin\theta \tag{3}$$

Lift Determination   In the cruise portion of the mission, the weight of the vehicle is known, we can determine the Coefficient of Lift required to support the vehicle. This is done using Equation 4.

$$C_L = \frac{\text{weight}}{q_\infty S} \tag{4}$$

Lift over Drag   The Lift to Drag Ratio is calculated using Equation 5. Lift over drag is a primary input into the Bergeut range equation that can be used later for estimating the range. The Lift to Drag ratio is plotted in Figure 3. The drag was optimized to be at its minimum at our cruise condition. With more time, the component build up method could be used to determine if this drag estimate is accurate.
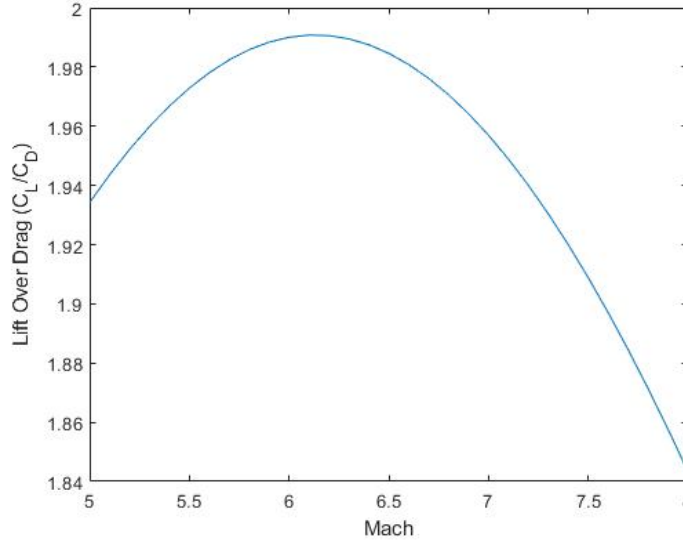
$$\text{Lift over Drag} = \frac{C_L}{C_D} \tag{5}$$

Figure 3: C_L/C_D v. Mach

3.3   Inlet, Isolator, and Compression Duct [Thomas Satterly]

Inlet   The inlet was designed to provide the desired mass flow rate (3.5 kg/s) at cruise conditions whilst being capable of starting at Mach 5.5. Additionally, the geometry must be axisymmetric in order for a smooth flowpath from the inlet to the RDE. To satisfy these constraints, a simple conical inlet with variable geometry was selected. A capture area of 452 cm^2 was needed to deliver the desired mass flow rate at cruise conditions, which resulted in a cowl outer diameter of 0.24 meters.

A cone with a half angle of 5 degrees was selected to minimize pressure loss and heat transfer at the inlet. By solving the Taylor-Maccoll equations for a conical shock, the outer cowl was sized to place the shock at the cowl during cruise conditions. In order to avoid mass flow loss and extra drag due to spillage at the starting conditions, a variable geometry cone is desirable to keep the shock at the cowl. This is achieved by shifting the inlet cone axially during acceleration. For this inlet to perform as desired between Mach 5.5 and 6.5, the cone only needs to be able to move 2.6 cm in total. The extremes of the cone position, as well as the shock placement on the cowl, can be seen in Figure 4.
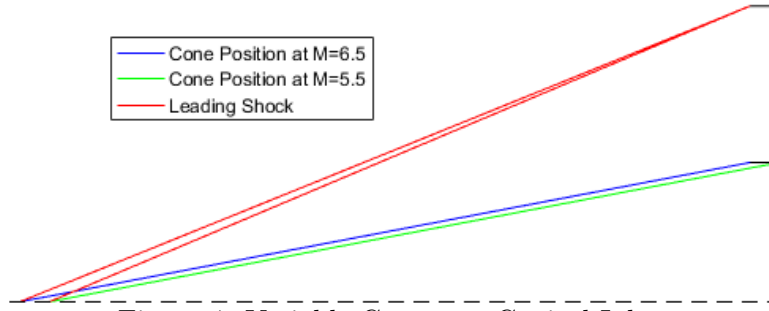
Figure 4: Variable Geometry Conical Inlet

Isolator The isolator was designed using a combination of industry accepted assumptions and correlations rather than a complete shock train analysis, given that this is a preliminary design. A constant area annular duct was chosen for the general geometry, as it would transition easily from the conical inlet and minimally disrupt the flow as it approaches the combustor. A major assumption made was that the exit Mach from the isolator is 1/2 of the entrance Mach to the inlet. Typically, this ratio is closer to 1/3, but a great advantage of the RDE is the possibility to maintain combustion at high Mach numbers. If this design exercise is to be forward-looking, it is not unreasonable to assume that more capable isolators will also be developed in the future. The total pressure ratio of the isolator is taken from MilStd 5007D [1], which is a relationship between free stream Mach and total pressure ratio that has been standardized to allow for preliminary design and sizing of an inlet and isolator system without spending valuable resources on an extensive flow analysis. Finally, the length of the inlet was derived using the Waltrup and Billig correlations [15]. The final isolator parameters are shown in Table 1.

Outer Diameter (m)	0.24
Gap Size (m)	0.0635
L/D	18
Mach Ratio	0.5
Total Pressure Ration	0.294

Table 1: Isolator Parameters

Compression Duct The final piece needed before reaching the combustor is a compression duct between the isolator and RDE entrance. The compression duct serves many purposes that ultimately balances the RDE operational properties with the upstream properties already set by the inlet and isolator system. The inlet sets the mass flow rate while the isolator sets the total pressure and Mach of the flow before reaching the compression duct. The RDE, on the other hand, was designed to operate at a specific static pressure, mass flow rate, and has a prescribed geometry. The compression duct unifies these components by delivering the flow from the inlet and isolator system, which have their own prescribed geometry, to the RDE such that flow properties are not violated. This was accomplished primarily by iterating on possible RDE operational conditions and geometry and verifying that, if the compression duct is isentropic, the upstream flow can be successfully delivered to the RDE within its design specifications. The length of the compression duct was determined primarily by packaging, and is roughly half of the length of the isolator. A cross section view of the inlet, isolator, and compression duct systems can be seen in Figure 11.

3.4 Combustor [Thomas Satterly]

The chosen combustor was a gaseous ethylene fueled RDE. The sizing of the combustion chamber was based off of the Bykovskii et. al.[4] guidelines and experimentally observed cell sizes for gaseous ethylene [3]. Chapman-Jouget detonation parameters were calculated using the NASA CEA program [8], and the RDE performance was analyzed using the model proposed by Stechmann [13]. The mass flow rate, minimum pressure, and minimum temperature were varied and the design iterated, along

with the inlet, isolator, and compression duct, until a reasonable and unified flow path was found with acceptable performance.

From experimental data collected by Bull et. al. [3], the approximate cell size of an ethylene-air mixture at 195 kPa is approximately 12.6 mm. From the guidelines given by Bykovskii in equations 6 through 9, the bounds on the RDE size can be calculated, where a is the cell size, d_c is the outer diameter, and Δ is the annulus gap.

$$h \cong (12 \pm 5)a \tag{6}$$

$$(d_c)_{min} = \frac{h(7 \pm 2)}{\pi} \tag{7}$$

$$L_{min} \cong 2h \tag{8}$$

$$\Delta \cong 0.2h \tag{9}$$

From these guidelines, the RDE outer diameter was chosen at 0.2035 m with an inner diameter of 0.16 m and a total length of 0.254 m. The RDE also employs regenerative cooling channels to ensure the combustor hardware does not melt during the mission. A CAD model of the combustor can be seen in Figure 5.
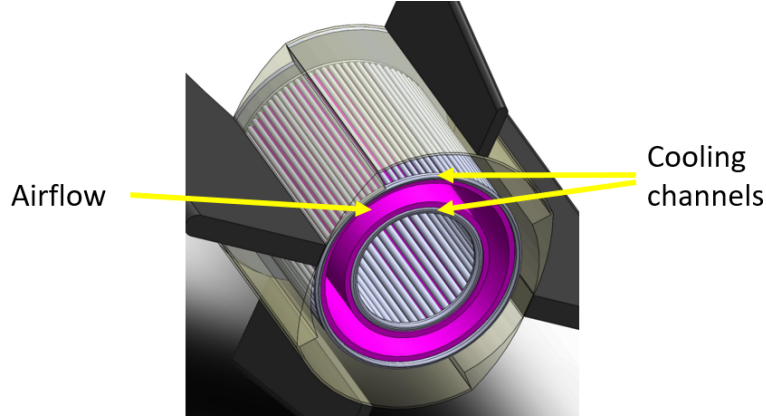

Figure 5: Combustor Geometry

Using the Stechmann model [13], the RDE's performance was analyzed across the flight conditions the vehicle would experience. During acceleration, an equivalence ratio of 1 was chosen to capitalize on performance while avoiding extreme temperatures. During cruise, the equivalence ratio was reduced to 0.58 in order to produce enough thrust for steady level flight. The performance characteristics of the RDE is shown in table 2.

	Acceleration	Cruise
Isp(s)	2131-2219	2080
Thrust (N)	3076-1963	1007.19
Air Mass Flog (kg/s)	3.868-3.346	3.346
Fuel Mass Flow (kg/s)	0.262 - 0.227	0.131
Cf	1.61 - 1.67	1.664
C* (m/s)	1444	1326
Eq. Ratio	1	0.58
CJ Pressure Ratio	5.327 - 5.11	4.25
CJ Temperature Ratio	2.93 - 2.84	2.54
Combustor Mach	1.5 - 2.14	2.14
Entrance Pressure (kPa)	250 - 195	195

Table 2: Performance Results

Figures illustrating the changing performance parameters between detonation fronts can be found in Appendix C.

A major assumption made in this model is the ability for an RDE to be able to deep throttle from an equivalence ratio of 1 down to 0.58. Such a shift will affect the cell size and impose transients during throttling, of which neither effect has been studied in detail and remains an important question for the true capability of an RDE. A cross section view of the combustor can be seen in Figure 6
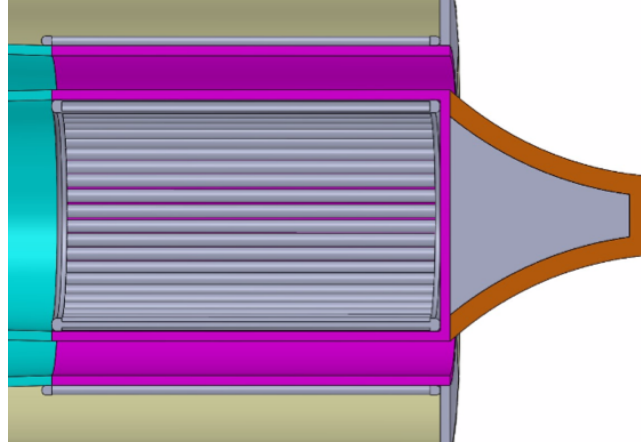

Figure 6: Combustor and Nozzle Cross Section

3.5   Nozzle [Gabriel Diez]

An aerospike nozzle design was chosen to expand the gases exiting the combustor and add additional thrust. Imbaratto [7] specifies a method to design the contour of an ideally expanded aerospike nozzle utilizing the Prandtl-Meyer function. The method starts by calculating the nozzle pressure ratio. Normally, nozzles are designed for a combustor with a constant chamber pressure, however, in an RDE engine the pressure varies with time and location as a result of the travelling detonation wave. Therefore, the average pressure over the whole nozzle entrance area was calculated to be 365.8 kPa. Based on this pressure and the combustor exit Mach number and temperature of 2.14 and 2417 K, respectively, the Prandtl-Meyer function was solved to find the maximum turning angle of the flow at several points. A MATLAB program was then made to plot these points, developing the nozzle contour along the axial length from the combustor.

The result of this is shown in Figure 7 and it is apparent that the ideal contour leads to a long and sharp tip. While this thin tip does lead to perfect expansion to ambient pressure, it is impractical for several reasons. Manufacturing a shrinking spike with a precise geometry such as this would be difficult and the pointed end could be easily damaged. The main problem with the purely ideal aerospike nozzle, however, is heat transfer. Developing a system to effectively remove the heat being deposited in a 2 mm diameter pointed spike by supersonic gas at the high temperatures exhibited by a scramjet would be far too strenuous to justify the negligible improvement in expansion it would provide. The static pres-
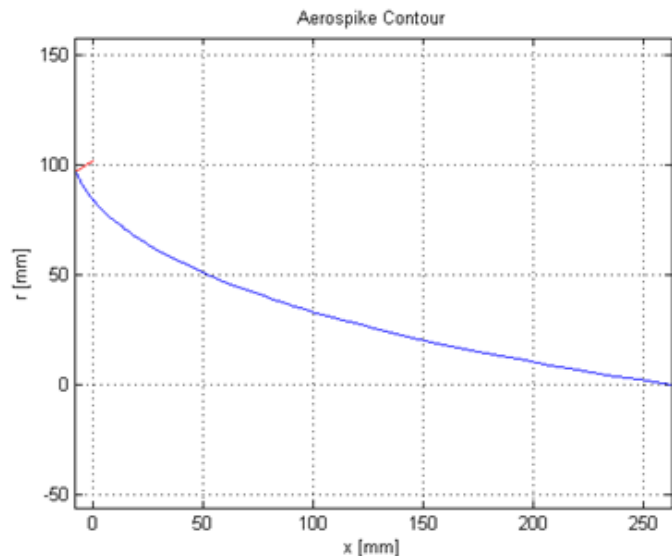

Figure 7: Aerospike Contour

7

sure as a function of distance long the
nozzle was then calculated and plotted
in Figure 8. A point 127 mm in length
and 25 mm in radius was chosen to truncate the nozzle as it would only leave the exiting flow with a
static pressure of about 3 KPa above ambient which was deemed acceptable. The final nozzle design
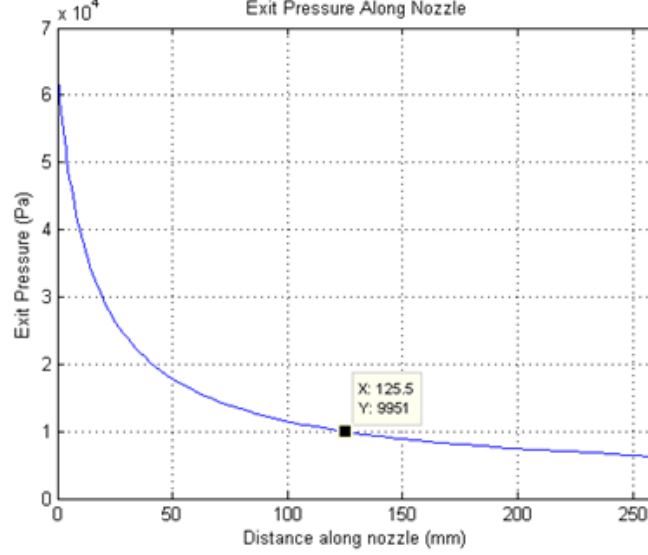is displayed in Figure 16.

Figure 8: Pressure Along the Aerospike

3.6 Heat Transfer

3.6.1 Combustor [Cameron Ellis]

The combustor consisted of a rotating detonation engine surrounded by an inner and outer wall that
were each coated in TBC and regeneratively cooled. Heat transfer through the walls was calculated
using a modified form of Bartz equation in order to calculate the heat transfer coefficient hg inside
the combustor. Equation 10 shows the standard form of Bartz equation for a rocket nozzle.

$$h_g = \left[\frac{0.026}{D_t^{0.2}} \left(\frac{\mu^{0.2} C_p}{Pr^{0.6}} \right)_{ns} \left(\frac{(p_c)_{ns} g}{c^*} \right)^{0.8} \left(\frac{D_t}{R} \right)^{0.1} \right] \left(\frac{A_t}{A} \right)^{0.9} \sigma \tag{10}$$

Where the ns subscript denotes values of the gas inside of the combustor, and where sigma is the
correction factor denoted by Equation 11.

$$\sigma = \frac{1}{\left[\frac{1}{2} \frac{T_{wg}}{(T_c)_{ns}} \left(1 + \frac{\gamma - 1}{2} M^2 \right) + \frac{1}{2} \right]^{0.68} \left[1 + \frac{\gamma - 1}{2} M^2 \right]^{0.12}} \tag{11}$$

For this combustor, there is no nozzle radius of curvature, denoted by R in the Bartz equation,
so the term $\left(\frac{D_t}{R} \right)^{0.1}$ becomes 1. Furthermore, the area of the throat and the area of the combustor
are equal since they have the same radius, so the area ratio term $\left(\frac{A_t}{A} \right)^{0.9}$ also becomes 1. Once an
hg value was obtained, a guess at the hot side wall temperature, T_{wg} was taken and used to calculate
heat flux from the combustor to the surface of the wall. This heat flux was then compared to the heat
flux from the liquid coolant to the cold side of the wall, and compared together. The hot side wall
temperature then changed iteratively until the two heat flux values matched. This was done across
the entire length of the combustor, and was used to find the temperatures of the TBC inside the
combustor, the temperature of the metal inside combustor wall, and the temperature of the ethylene
in order to make sure boiling would not occur.

Figure 9 shows the temperature of the TBC, inside metal wall, and the ethylene across the length of the combustor. The TBC experiences temperatures of upwards of 1327 K at the hottest points after regenerative cooling is applied. The metal wall experiences up to 930 K, and therefore a material that could withstand those temperatures without going past its deformation temperature had to be selected. Incoloy 800 HT was chosen due to its high heat resistance. At the calculated temperatures, the alloy would be able to work at about 60% of its intended strength. The TBC coating selected was NAS3-23944, a super TBC created by NASA.

Figure 15 displays the elongation, tensile strength, and yield strength for INCOLOY 800HT for various temperatures. Though at the temperatures the RDE combustor would be operating at would affect the strength of the INCOLOY, it is still within a reasonable operating range for the metal work as intended.

Figure 9: Temperature Range Across Combustor Structure

To regeneratively cool both sides of the combustor, the mass flow rate of the liquid ethylene had to be split up between the inner and outer walls. Since the inner wall has a lower surface area, it would need less cooling channels, while the larger outer wall would need more. The cooling channels were split into 100 channels on the inner wall and 120 channels on the outer wall. Each cooling channel has a dimension of 0.215"x0.125" The mass split of the fuel ended up being 48.5% of fuel going to the inner regenerative cooling, and 51.5% of fuel going towards the outer regenerative cooling. This allows the two walls to experience approximately the same heat transfer, so the same thickness of thermal barrier coating would be able to be used on both sides. This was done to ensure that one side would not need to thick a layer of thermal barrier coating and increase the chance of cracking and flaking to take place during combustion.

3.6.2 Nozzle [Gabriel Diez]

The data used to design the ablative cooling system on the nozzle was taken from Tick et al [14]. In the study N2O4 and hydrazine were burned at 830 kPa and exhausted out of a nozzle coated with a 12.5 mm thick layer of silica phenolic ablative. Several parameters were varied in the experiment but in each test the fluid temperature exiting the combustor was 3144 K which lead to surface temperatures on the nozzle of 2644 K. Under these conditions, the time to char through the ablative as well as the erosion rate were measured. The time to char through was above 200s and the erosion rate never exceeded 0.05 mm/s. Since the total burning time of the RDE scramjet is 120 s and the gas temperatures never exceed 2500 K, it can be estimated that no more than 6 mm of ablative will be burned off. Therefore a design with a 12.5 mm thick layer of silica phenolic ablative coating similar to the one used in the Tick et al [14] study was chosen since it had been proven experimentally to function under harsher conditions for a longer period of time. The ablative coating covers a metal interior support made of titanium for even further protection against any conductive heat transfer. A cross section of the ablative layer is displayed in Figure 6.
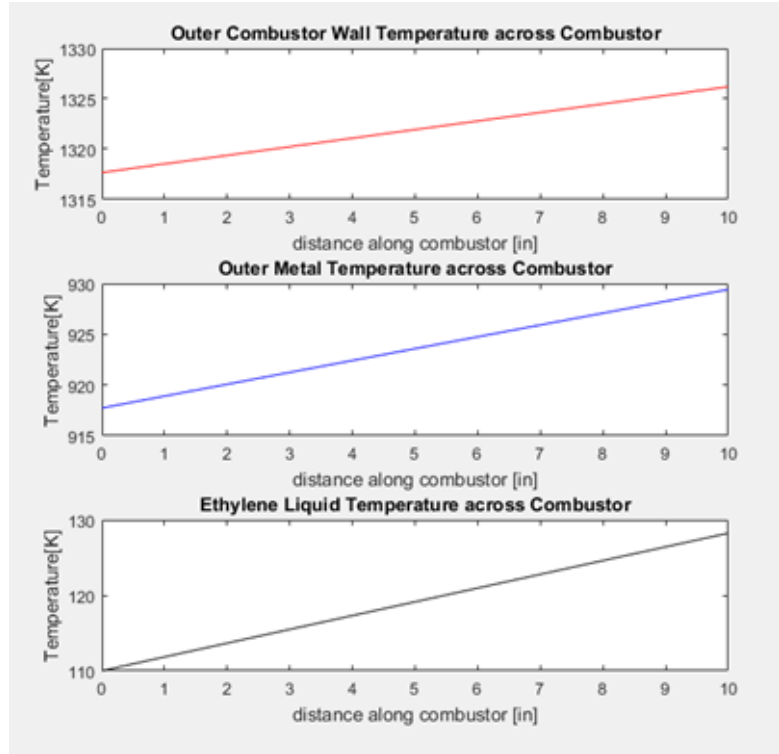
9

3.6.3 Wings and Leading Edges [Alberto Marin Cebrian]

All the temperatures have been calculated for the steady state and for the most demanding operating conditions (cruise, Mach 6.5). The materials used in these exterior surfaces must tolerate high temperatures and a high emissivity is desirable. A higher emissivity will allow the material to reduce the maximum temperature it will have to withstand because it will be able to radiate more heat to the surroundings.

Inlet Cone Tip and Wing Leading Edges Infinitely thin surfaces and points are not possible to manufacture. Due to this fact a small normal shock will appear in front of these blunt bodies. This detached normal shock will create a huge deceleration of the flow and the properties of the flow will change significantly, it has been assumed that the air properties (γ in particular) will also change as the flow crosses the shock.

Properties after the shock allow us to calculate the Prandtl number at that location

$$Pr = \frac{(\mu_e Cp_e)}{K_e} = 0.4574 \tag{12}$$

Assuming that the boundary layer remains laminar, a similarity solution exists.

$$\frac{du_e}{dx} = \frac{1}{r_n}\sqrt{\frac{2(p_e - p_0)}{\rho_e}} \tag{13}$$

The recovery temperature depends on the Prandtl number. For laminar flows the recovery factor is r=sqrt(Pr)

$$T_r = T_e(1 + (\gamma_e - 1)/2\sqrt{Pr}M_e^2) = 2082K \tag{14}$$

Convective heat flux on the inlet cone tip The shape of the blunt cone is approximated to a semi-sphere. The heat flux is given by:

$$\dot{q} = 0.763Pr^{0.6}(\rho_e\mu_e)^{1/2}\sqrt{\frac{du_e}{dx}}Cp_e(T_r - T_w) \tag{15}$$

Convective heat flux on the wing leading edge The leading edge of the wing has a cylindrical shape with a nose radius equal to half of the thickness of the wing. The heat flux is also given by given by Equation 15.

Radiation heat flux The radiation heat flux has been calculated with the Stefan-Boltzman equation.

$$\dot{q}_{rad} = \sigma_s(\eta_w T_w^4 - T_0^4) \tag{16}$$

The steady state solution is reached when $\dot{q} = \dot{q}_{rad}$.

	Inlet Cone Tip	Wing Leading Edge
Nose Radius (m)	$1*10^{-3}$	$1.27*10^{-2}$
Temperature (K)	1962	1435
Material	Tantalum	Nichrome
Maximum Operating Temperature	3023	1573
Emissivity	0.225	0.89

The cone tip radius value has been estimated and based on the manufacturing tolerance it may change significantly. On the one hand, a bigger nose radius will decrease the temperature of the cone tip but it will decrease the performance of the inlet adding more drag. On the other hand, a smaller nose radius will be beneficial for the inlet peformance but it will increase the temperature of the inlet cone. This value must be small enough not to affect significantly the inlet performance but big enough to be manufactured and get a temperature that lies inside the operating range of the material.

Wing Surface Temperature In order to obtain the temperature field over the wing of the aircraft the following assumptions have been made. The angle of attack of the vehicle is very small during the flight. This fact allows us to simplify the physics of the problem assuming that the angle of attack (α) is zero. In reality the angle will be different from zero and a compression oblique shock wave will appear for the lower part of the wing and an expansion wave will be developed in the upper surface. These waves will be very weak and will not change significantly the results of this analysis as soon as the angle of attack keeps being small enough. The wings are long and slender. Flat plate approximation has been used to calculate the heat fluxes at different sections of the wing. 1-D flow. The velocity of the flow can be simplified to $\overrightarrow{v} = (u, 0, 0)$.

Some important non-dimensional parameters that control the physics of this problem are the Reynolds number, the Prandtl number and the Nusselt number. The Reynolds number , Equation 21, relates the inertial and viscous effects. It determines the change from laminar to turbulent flow in the boundary layer. For a flat plate, the transition Reynolds number from laminar to turbulent is 500,000.

The Prandtl number, Equation 22, is a dimensionless parameter representing the ratio of diffusion of momentum to diffusion of heat in a fluid.

The recovery factor (r) depends on both, Prandtl number and Reynolds number.

$$r = \sqrt{Pr} \text{ For laminar B.L.}$$
$$r = Pr^{1/3} \text{ For turbulent B.L.}$$

(17)

The Nusselt number, Equations 23, is the ratio of convective hat transfer with respect to conduction. The Nusselt number can be rewritten to depend on the other two dimensionless parameters (Prandtl number and Reynolds number) in Equation 18.

$$Nu_x = 0.332\sqrt{Re_x}Pr^{1/3} \text{ For laminar flows}$$
$$Nu_x = 0.0296Re_x^{0.8}Pr^{1/3} \text{ For turbulent flows}$$

(18)

With the Nusselt number and the axial position it is possible to obtain the convective heat transfer coefficient h_g.

$$h_g = \frac{KNu_x}{x}$$

(19)

Note that this analysis is not valid for x=0 where the leading edge is located (h_g is infinite there). The convective heat flux is

$$\dot{q} = h_g(T_r - T_w)$$

(20)

Steady state is reached when the heat dissipated by radiation equals the heat inflow due to convection $\dot{q} = \dot{q}_{rad}$ In order to get the temperature contour of the wing, the wall temperature of the wing has been calculated in numerous locations along the wing.

3.7 Turbopump and Tank Sizing [Drew Sherman]

With cooling a serious issue in hypersonic aircraft, significant attention must be paid to the coolant used and its conditions. For the regenerative cooling system required by the aircraft's extreme thermal conditions, it becomes important to understand how the fuel, ethylene, behaves as it cools. One tactic used to ensure predictable and safe cooling is keeping the fuel above its critical point. Ethylene's critical point is about 5 MPa. Keeping coolant above its critical point theoretically eliminates boiling/two-phase flow concerns as the fuel is pumped over hot material, absorbing heat. The extreme pressure ensures that the liquid will not boil, even in extremely hot environments, which may or may not be seen. Unfortunately, keeping ethylene at this high of a pressure requires a significant initial pressurization and heavy tanks or an active pressurization system on the craft, operating during flight. A simple trade study was used to determine which method should be used to minimize overall system mass.

It is popular to load the fuel into craft at high pressure, which may be feasible depending on the margin allowed for tank weight. Tank weight is dependent upon the mass and density of the fuel stored and the pressure desired for the fuel in the tank. Standards from ASME [12] indicate a burst pressure of approximately three times storage pressure, which must be reflected in the weight. According to given conditions, the fuel tanks can achieve a ratio of $PV/W = 1e6in$. The sizing parameters of the turbopump and listed in table 3.

	Value (SI)	Value (Imperial)
Ethylene Mass	21 (kg)	46.3 (lbm)
Tank Burst Pressure	21 (MPa)	3045 (psi)
Ethylene Storage Pressure	7 (MPa)	1015 (psi)
Ethylene Density	567.7 (kg/m^3)	0.02051 (lbm/in^3)
Tank Mass	3.2 (kg)	6.9 (lbm)

Table 3: Turbopump Sizing Parameters

Initial aircraft sizing and design was based on a small turbopump system that was designed based on parameters from a paper developed by Blank et. all at Purdue University [2]. Figure 10 illustrates the major componenets of the turbopump system.
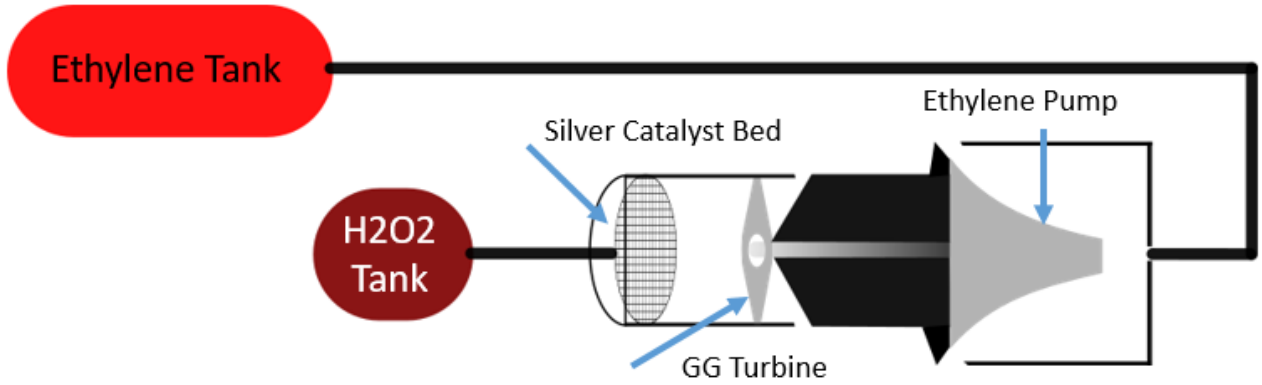

Figure 10: Turbopump System Illustration

The turbopump is driven by liquid rocket-grade (90%) hydrogen peroxide (lH2O2) . Sending the peroxide through a silver catalyst bed allows for decomposition and combustion. The products are sent through a small turbine used to drive a pump, raising ethylene pressure. The model is based off catalyst bed loading values and pressure drop values from Blank's paper [2]. The model uses NASA Chemical Equilibrium Analysis (CEA) to calculate the performance of the silver gas generator at various operating pressures. The rest of the system assumes certain pressure drops, including piping, cooling, and injection pressure losses. Using known and desired conditions for the ethylene, the model solves for the required peroxide massflow to run the pump at various operating pressures by balancing power requirements. Figure 17 in Appendix A shows the relationship between gas generator operating pressure and required massflow.

As can be seen, gas generator chamber pressure affects the amount of peroxide required to drive the pump, but the peroxide massflow is still low. As such, its possible to run the gas generator at low chamber pressures to reduce chances of failure. In addition to solving for massflow, the model generates approximate sizing specifications required for the ethylene pump impeller given assumed performance requirements [5]. Given the relatively high performance of the pump, a strong material that can withstand low temperatures and high pressures is required. Research into rocket-grade turbopumps [9] shows that RENE 41 should be used for the walls and structure of the gas generator, turbine, and pump assembly due to its high-temperature capability and small thermal expansion[2]. The impeller. since it is estimated at spinning around 30,000 rpm, requires a strong material capable of handling low temperatures. Thus, a titanium alloy containing 5% aluminum and 2.5% tin is used, as it is capable of

handling the temperature range and intermediate reactive products from the gas generator [5]. Sizing and performance characteristics of the gas-generator turbopump system are listed in table 4.

Fuel Flowrate (kg/s)	0.13
H_2O_2 Flowrate (kg/s)	0.004
Total H_2O_2 Mass (kg)	0.75
Fuel dP (kPa)	7000
H_2O_2 Combustion Pressure (kPa)	345
Impeller Exit Radius (cm)	6
Impeller Inlet Radius (cm)	0.5
RPM	30,000
Wall Material	RENE 41
Iimpeller and Turbine Material	Titanium Alloy
Mass (kg)	5.3
Required Bed Area (cm^2)	0.15
Bed Loading (lbm/s/in^2)	0.4
Operating Power (HP)	3.2

Table 4: Turbopump Operational Parameters

The turbopump system is similarly sized to a typical turbocharger in a car, with higher performance.

With both pressurization methods analyzed, it becomes obvious that simply storing the ethylene at supercritical pressure results in less mass and less complexity. The turbopump assembly also takes up valuable volume in the center of the craft, which can be used for more fuel to extend range capability. If the required ethylene mass were to approximately double, the turbopump system begins to show its strengths. This is made apparent because tank mass increases linearly with fuel mass, while the turbopump system mass will only increase from the extra hydrogen peroxide required.

4   Mass Breakdown

To estimate the mass of the vehicle, multiple approaches were used. For generic structures, such as aerodynamic surfaces, the fuselage, and internal support, the weights were scaled by aerodynamic reference area from the results presented in the AFRL GHV concept. The avionics mass does not scale with vehicle size, and so was taken directly from the AFRL paper [10]. Specific component masses, such as the isolator and combustor, were estimated based on the geometry and materials used. The resulting mass breakdown can be seen in Table 5.

System	Mass (kg)	Mass Fraction (%)
Fuselage & Support	70.2	24.2
Tanks (Empty)	3.2	1.1
Ballast	18.0	6.2
Fuel	21.0	7.2
Avionics	133.6	46.1
Inlet	7.1	2.5
Isolator	14.3	4.9
Compression Duct	7.4	2.5
Combustor	13.8	4.7
Nozzle	1.6	0.5
Total	**290.2**	

Table 5: Mass Breakdown

5 Results

Performance parameters of the aircraft throughout the mission are listed on Table 6. The final designed flight path begins with the GO1 accelerating the aircraft to Mach 5.5 and an altitude of 25.33 km. At that point the engines will ignite and initiate a 62.5 s acceleration period until the cruising Mach number of 6.5 is reached where it will maintain speed for 45 seconds. The combined acceleration and cruising phases produce a range of 197.15 km for this mission. The thrust and specific impulse were calculated for the duration of the mission and plotted on Figure 12. During the acceleration portion of the flight the equivalence ratio is highest in order to produce maximum thrust, leading to steadily increasing specific impulse. Once the aircraft reaches the cruising Mach number, the equivalence ratio is lowered so that the thrust can be balanced with the drag, which leads to a sudden drop in Isp. While the calculated mass of 296.3 is slightly above the 273 kg maximum of the GO1 launcher, the mass of the avionics components was taken from the AFRL's GHV release [10] and could not be fully designed. In application, the avionics would most likely weigh less, as the mission for the GHV was significantly more complex than this design. A cross section of the vehicle as well as flow conditions during cruising speed are displayed in Figure 11.

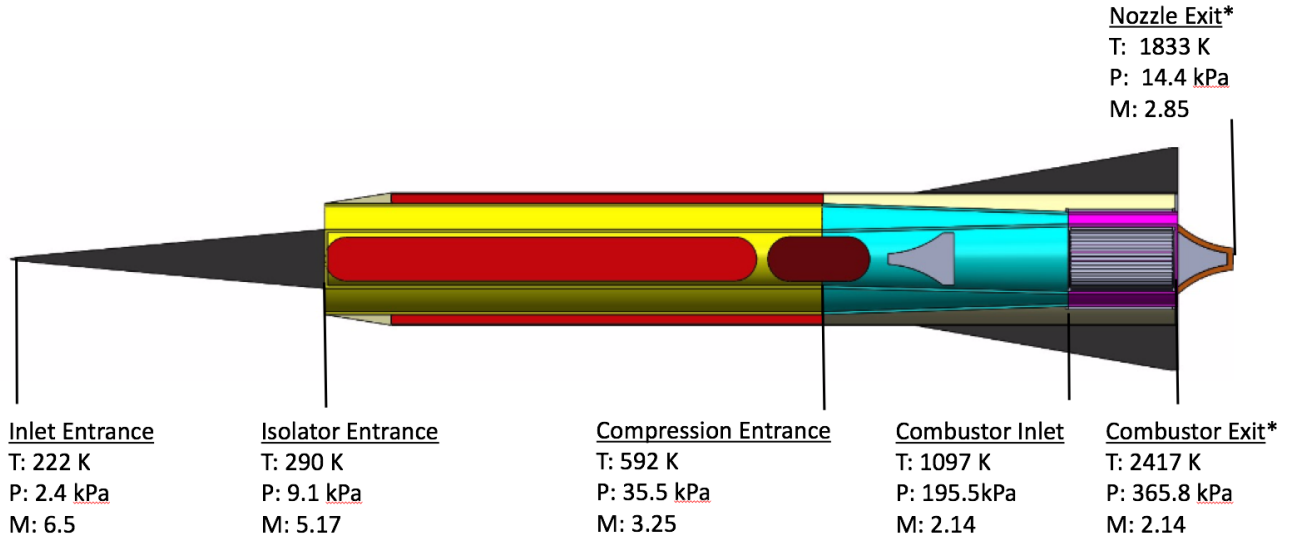| Key Performance Parameters	
Range (km)	197.15
Starting Mach	5.5
Cruise Mach	6.5
Cruise Altitude (km()	25.33
Acceleration Time (s)	62.5
Cruise Time (s)	45
Fuel Weight (kg)	21
Gross Weight (kg)	296.3
L/D	2

Table 6: Performance Results

Figure 11: Flow Station Parameters

During cruise, flow will enter the diffusor at Mach 6.5 a static pressure and temperature of 2.4 kPa and 222 K, respectively. The conical diffusor will vary its lateral position such that 5° half angle of the cone will produce an oblique shock that terminates at the cowl lip at the full range of Mach numbers for optimum pressure recovery. The oblique shock slows down the flow to Mach 5.17 and raises static pressure to 9.1 kPa. The flow then travels through an isolator. The isolator was designed

to produce a pressure ratio based on the MilStd 5007D [1]. Because of the higher combustor inlet Mach numbers RDE's are capable of operating at, the exit Mach number of the isolator is 3.25 and the static pressure and temperature is 35.5 kPa and 593 K, respectively. The parameters to produce a stable rotating detonation wave within the combustor are highly dependent on the area and entrance pressure of the burner. As a result, a transition is needed to unify the isolator exit and combustor entrance. A compression duct was then added to the design in order to guide the flow to the necessary area as well as raise the static pressure. This isentropic compression raises the static pressure to 195.5 kPa and the static temperature to 1097 K.

The ethylene fuel flows from the tanks within the center of the fuselage as well as the exterior of the fuselage through a regenerative heat exchanger that cools the combustor. In order to prevent film boiling in the regenerative heat exchanger, the fuel has to be above supercritical pressure. Consequently, upon injection, the fuel will flash vaporizes. In order to achieve these high pressures, ethylene is stored at 7 MPa, or 40% above its critical pressure. If there was approximately twice the amount of fuel on the craft, a hydrogen peroxide gas generator and turbopump could be employed to boost low-pressure ethylene above its supercritical conditions. Once the ethylene enters the combustor it mixes with the air flow and enables a rotating detonation wave that leads to an average static pressure of 365.8 kPa

Figure 12: Thrust and Isp v. Time

and static temperature of 2417 K. The Mach 2.14 flow exiting the combustor then flows through an ablatively cooled aerospike nozzle that expands the gases to 14.4 kPa and a final exit Mach number of 2.85. Figure 12 illustrates the vehicle performance over its entire mission.
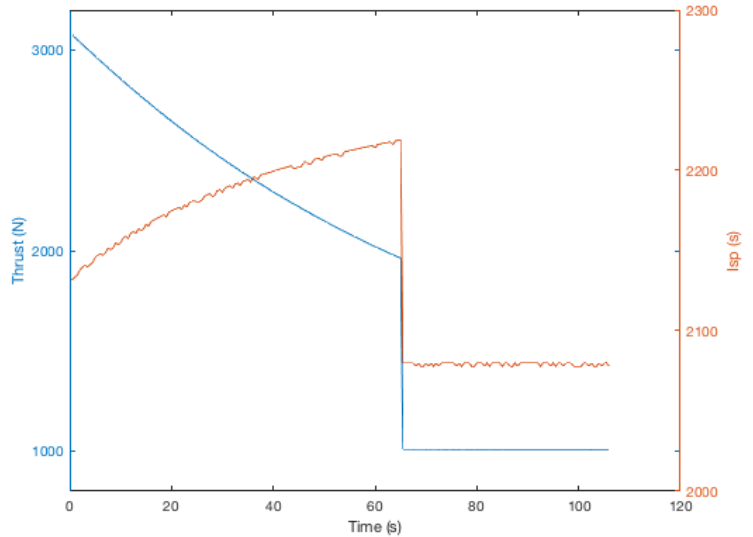
6   Conclusions

Overall, the use of an RDE on a hypersonic vehicle seems very promising, as it is predicted to deliver twice the Isp of a conventional scramjet. Additionally, the flameholding capabilities inherent to an RDE allow for combustion at higher Mach numbers, extending the range of capability for an RDE. However, there still remains many unanswered questions. For example, there is no good method for controlling the number of detonation fronts present in an RDE, which will effect performance. Additionally, deep throttling of the RDE is necessary to transition between acceleration and cruise conditions. This could cause many combustion stability issues due to the change of detonation cell size as the equivalence ratio changes, and the transients involved with throttling and RDE have not been deeply explored as of yet.

This design could also use more refined and in depth analysis to verify performance. The isolator was only analyzed using well known correlations, but due to the optimistic Mach ratio of the inlet and isolator system, a full shock train analysis should be performed to better characterize such a design. In the regenerative cooling jackets used on the RDE, the changing properties of supercritical ethylene need to be accounted for in order to verify that the combustor lining will not melt.

Once the above issues have been addressed, there will no doubt be interest in a larger scale hypersonic vehicle that could, itself, carry a payload. As the design scales up, many new opportunities present themselves. For instance, the fuel mass fraction is expected to increase, which will start to push the weight advantage towards storing fuel at low pressure and using a turbopump system to take the ethylene to supercritical conditions. Additionally, the RDE may not have to throttle at such large extremes, as a similarly sized RDE will still have enough thrust to power larger vehicles.

7 References

[1] MilStd 5007D.
General specification for engines, aircraft, turbojet, and turbofan, October 1973.

[2] R. A. Blank, T. L. Pourpoint, S. E. Meyer, S. D. Heister, and W. E. Anderson.
Experimental and Theoretical Performance of High-Pressure Hydrogen Peroxide Catalyst Beds, volume 28.
Journal of Propulsion and Power, 2012.

[3] D. C. Bull, J. E. Elsworth, P. J. Shuff, and E. Metcalfe.
Detonation Cell Structures in Fuel/Air Mixtures, volume 45.
Combustion and Flame, 1982.

[4] Fedor A. Bykovskii, Sergey A. Zhdan, and Evgenii F. Vedernikov.
Continous Spin Detonations, volume 22.
Journal of Propulsion and Power, November 2006.

[5] A. Csomor and R. Sutton.
Small, High-Pressure Liquid Hydrogen Turbopump.
Rockwell International, Canoga Park, CA, May 1977.

[6] Go1 overview, November 2017.

[7] David Michael Imbaratto.
The interaction between throttling and thrust vectoring of an annular aerospike nozzle.
mathesis, California Polytechnic State University, September 2009.

[8] Chemical equillibrium with applications.
https://www.grc.nasa.gov/www/CEAWeb/.
Accessed on 2017-12-17.

[9] NASA, editor.
Liquid Rocket Engine Centrifugal Flow Turbopumps.
NASA SP-8109, December 1973.

[10] Brent Ruttle, Jacob Stork, and Glenn Liston.
Generic Hypersonic Vehicle for Conceptual Analyses.
Air Force Research Lab, 2012.

[11] Incoloy alloy 800h & 800ht.
http://www.specialmetals.com/assets/smc/documents/alloys/incoloy/incoloy-alloys-800h-800ht.pdf.
Accessed: 2017-12-15.

[12] Walter J. Sperko.
Reduction of design margin ("safety factor") in the asme boiler and pressure vessel code in the 1999 addenda.
Sperko Engineering, June 2000.

[13] David Stechmann.
Performance Analysis.
Purdue University, 2017.
Provided by Dr. Heister's AAE 53700 course materials.

[14] S. J. Tick, G. R. Huson, and R. Griese.
Design of Ablative Thrust Chambers and Their Materials, volume 2.
AIAA Journal, May 1965.

[15] P. J. Waltrup and F. S. Billig.
Structure of Shock Waves in Cylindrical Ducts, volume 11.
AIAA Journal, 1973.

[16] Chang-Hui Want, Yu Lui, and Li-Ze Qin.
Aerospike Nozzle Contour Design and its Performance Validation.
ACTA Astronautica, January 2009.
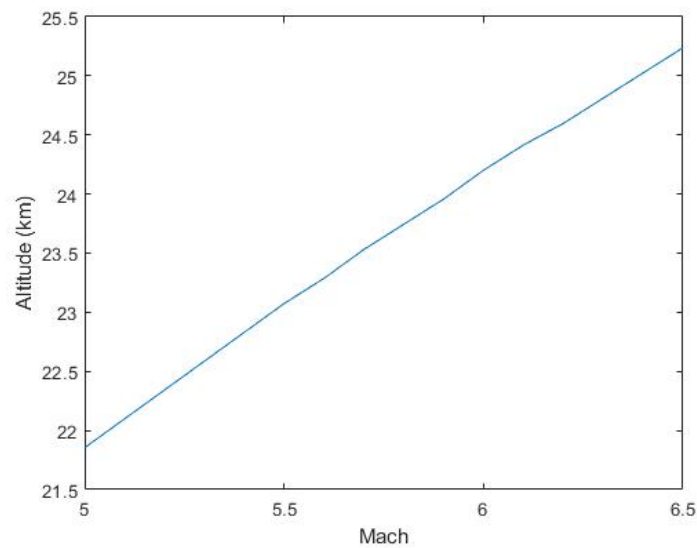
8   Appendix A: Figures
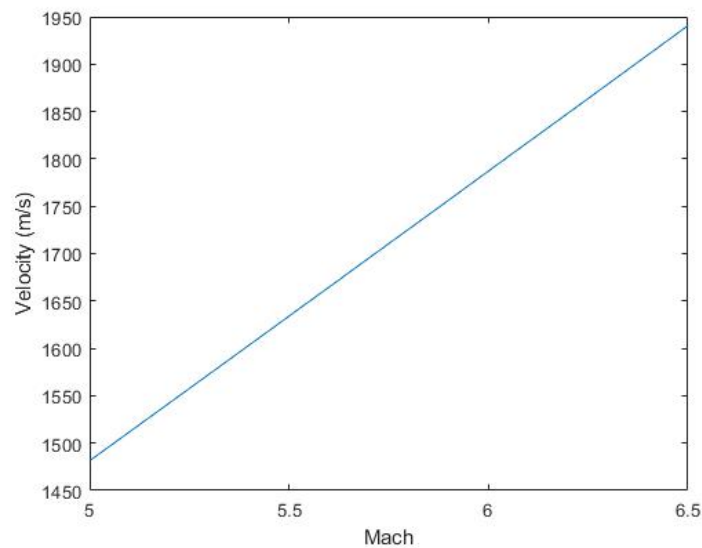

Figure 13: Altitude v. Mach
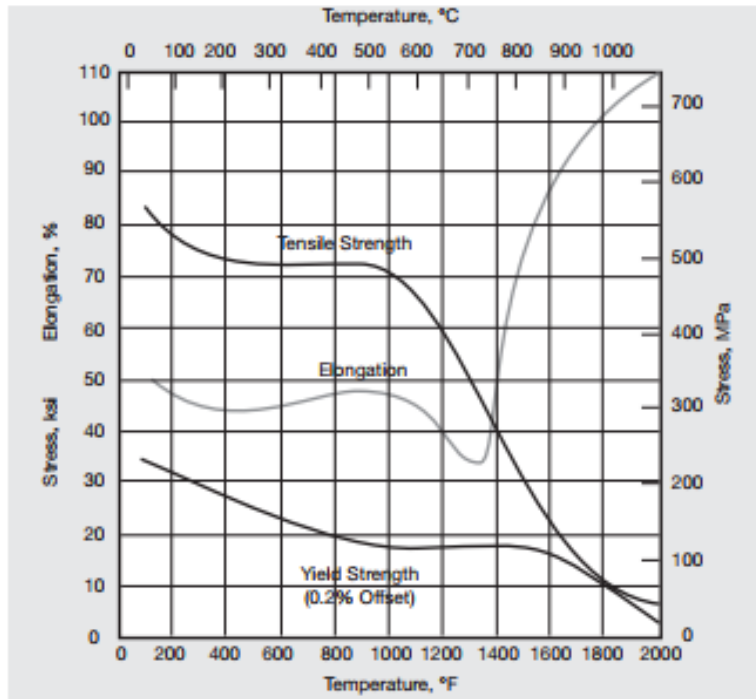

Figure 14: Velocity v. Mach

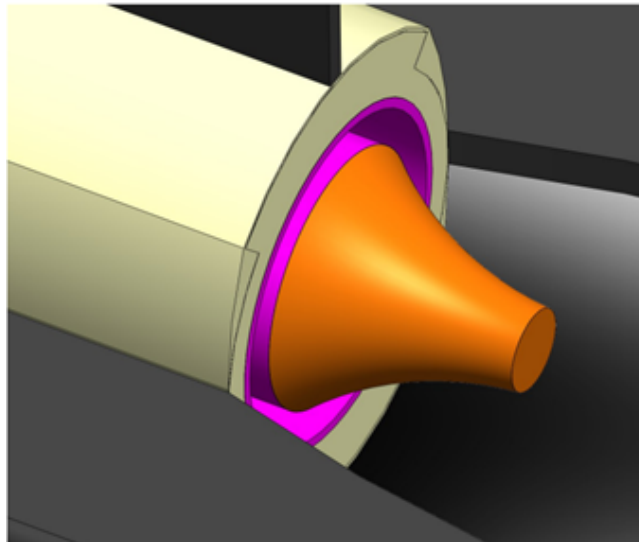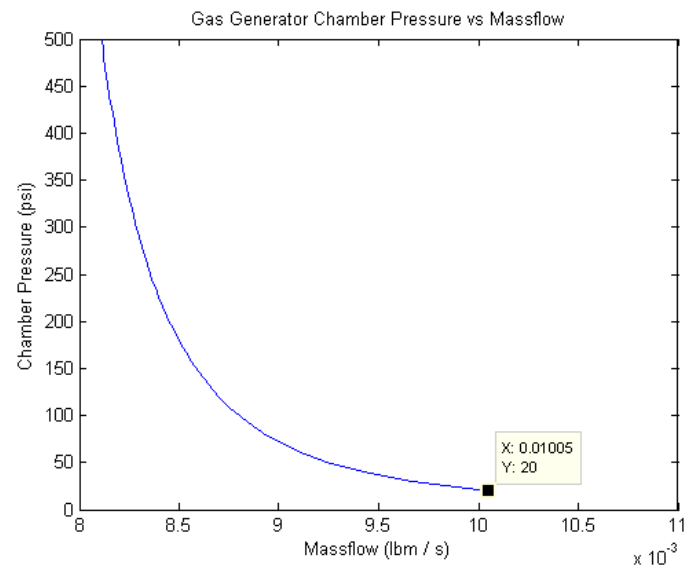Figure 15: Temperature Range Across Combustor Structure [11]

Figure 16: Final Nozzle Design
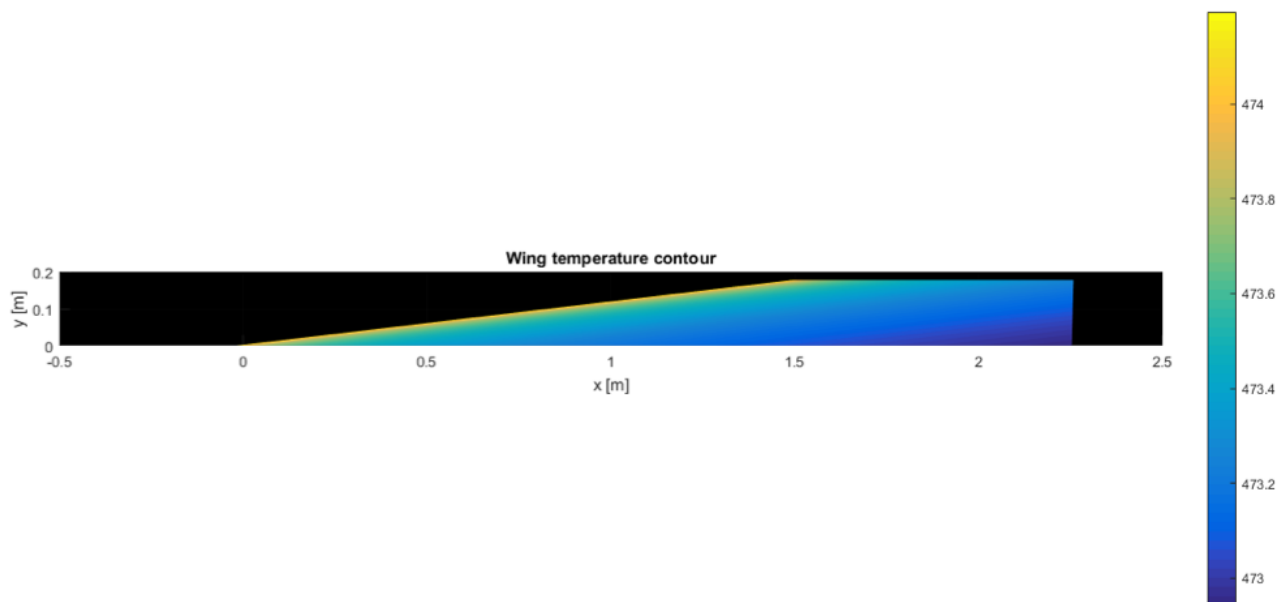
Figure 17: Turbopump Pressure v. Mass Flow Rate

Figure 18: Wing Surface Temperature Plot

9 Appendix B: Additional Equations

$$Re_x = \frac{\rho u x}{\mu}$$

If $Re_x < 500,000,$ Laminar boundary layer

If $Re_x > 500,000,$ Turbulent boundary layer

$$(21)$$

$$Pr = \frac{\mu Cp}{K} \tag{22}$$

$$Nu_x = \frac{h_g x}{K} \tag{23}$$

$$Re_x = \frac{\rho u x}{\mu}$$

10   Appendix C: RDE Performance Figures
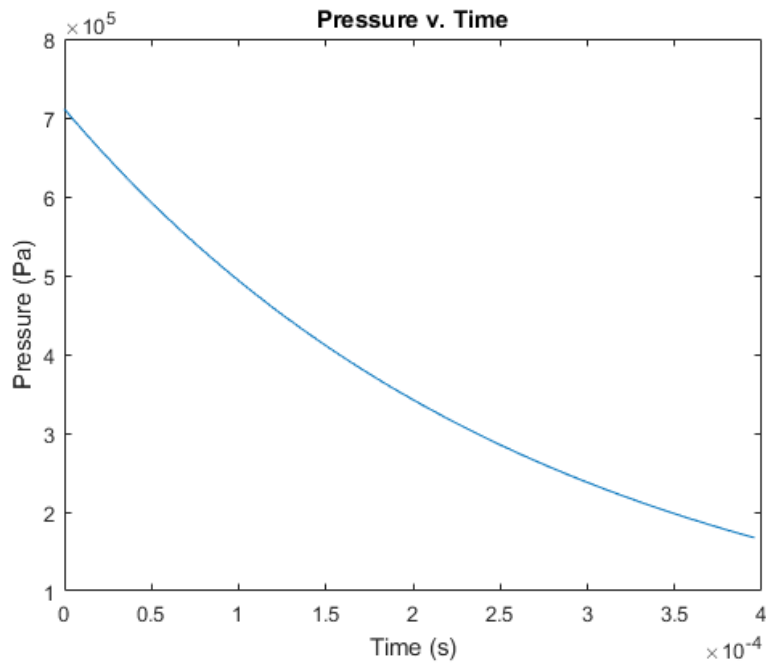
Figure 19: Pressure v. Time
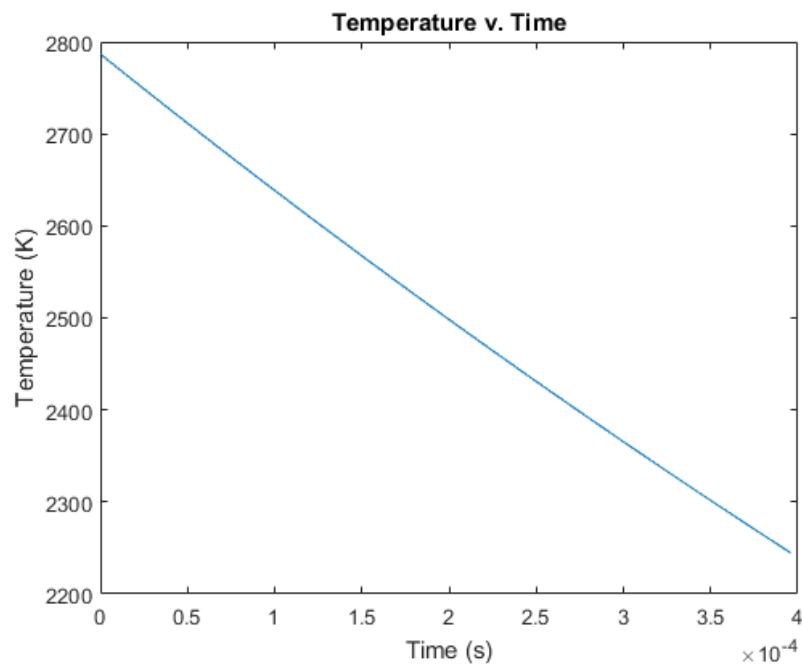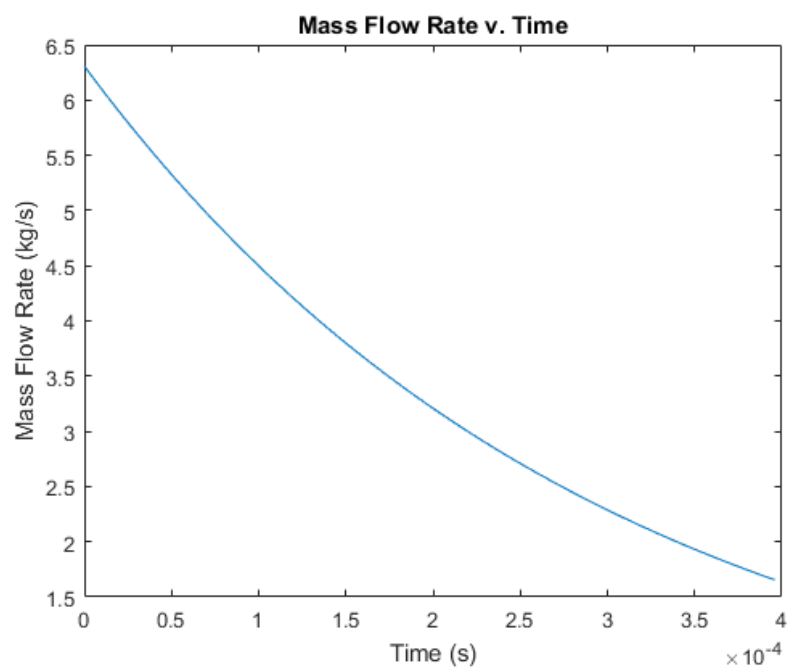

Figure 20: Temperature v. Time
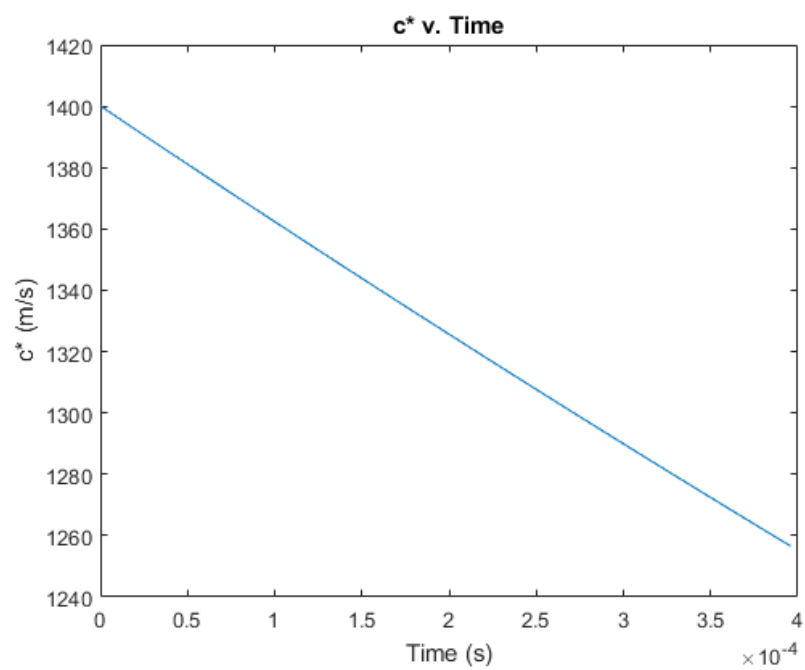
Figure 21: Mass Flow Rate v. Time
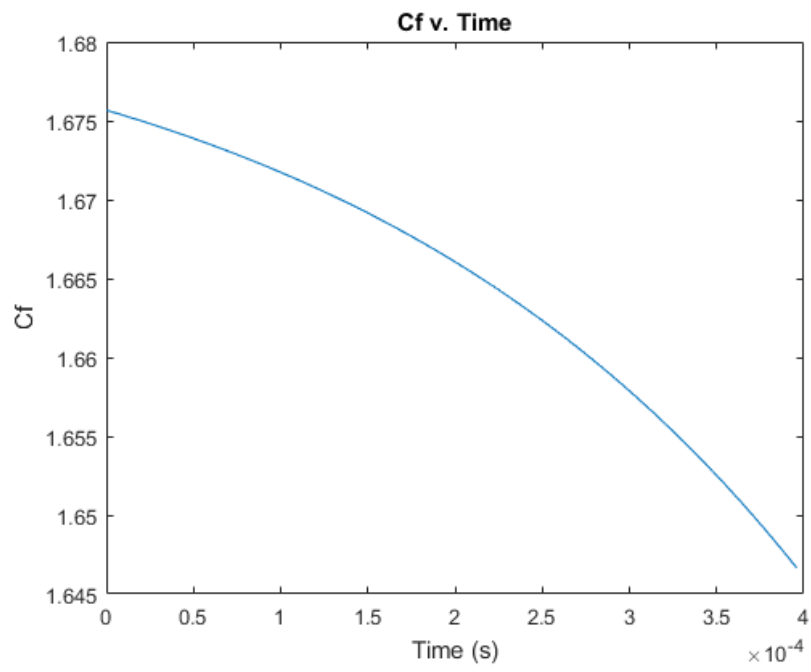

Figure 22: c^* v. Time

Figure 23: Cf v. Time
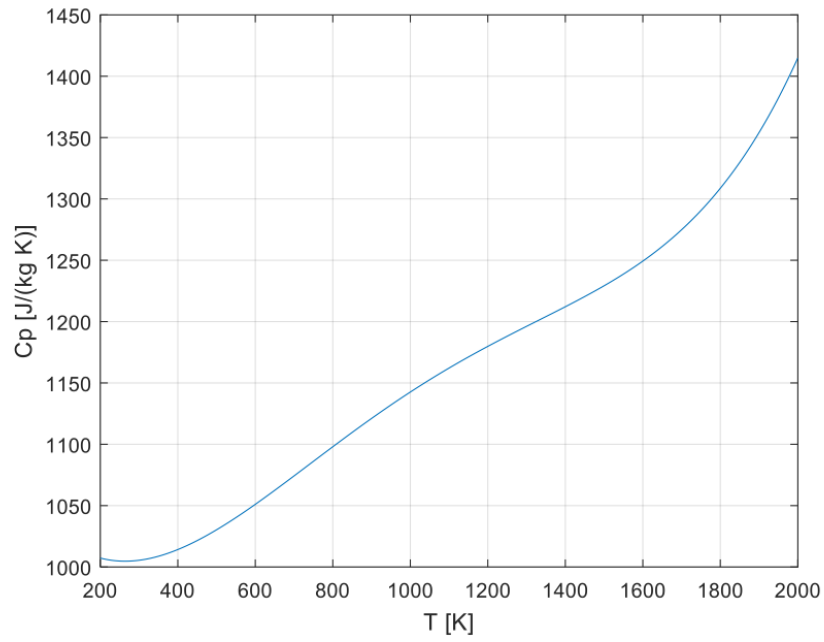
11   Appendix D: Air Properties

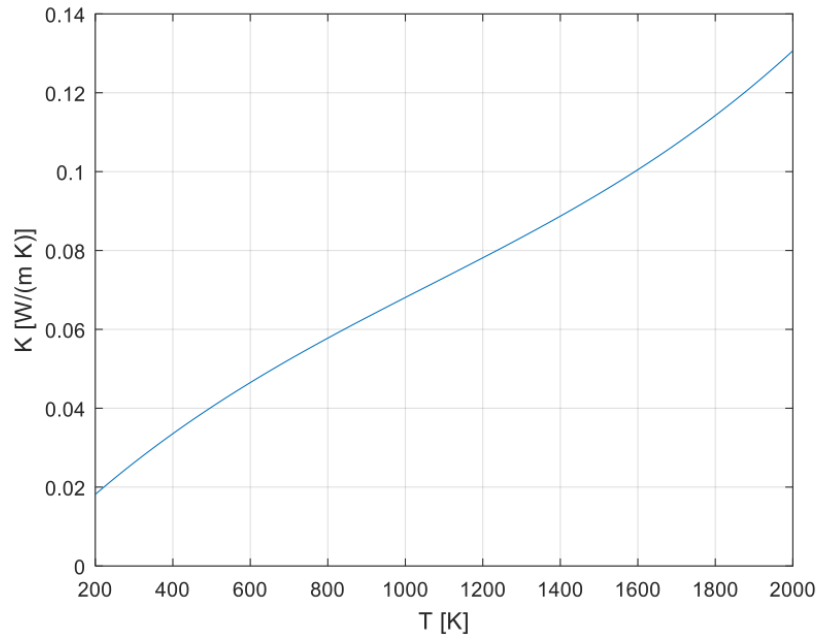Figure 24: Specific Heat v. Temperature for Air

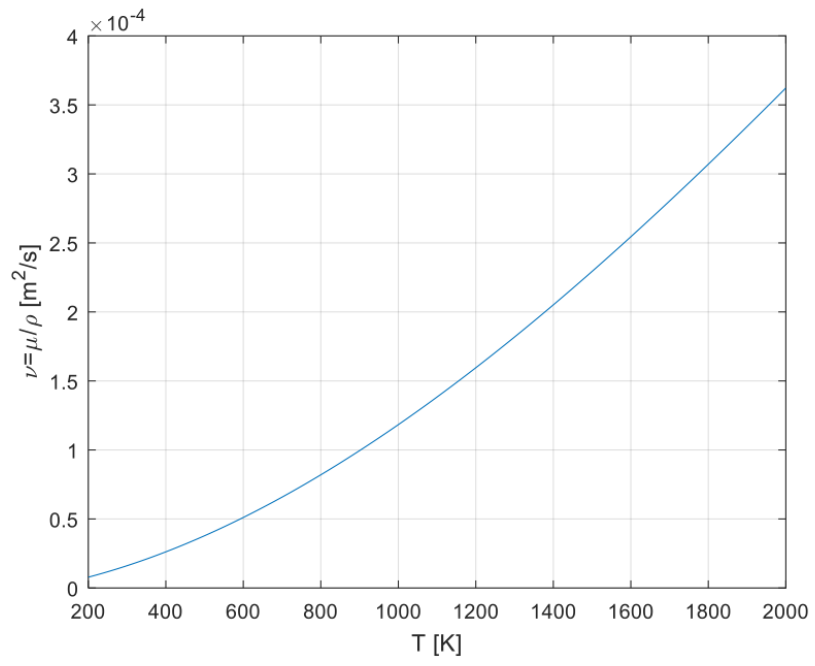Figure 25: Conduction Heat Transfer Coefficient v. Temperature for Air

Figure 26: Kinematic Viscosity v. Temperature for Air

12 Appendix E: Chapman-Jouguet Detonation Model

This page intentionally left blank

Before having available the Matlab version of the NASA CEA computer program, the properties of the flow after a Chapman-Jouguet detonation were obtained using a Matlab code based on this simple model.

The CJ detonation was modeled as a shock wave followed by a heat addition region. A sketch of this detonation model can be seen in Figure []
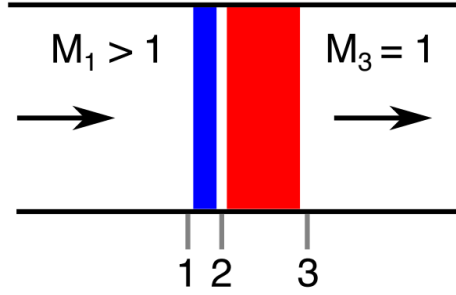

Figure [2], the shock wave is blue and the heat addition zone is red (from [3])

The problem is solved from the shock wave reference frame. However, the inertial forces that may appear due this change to a relative reference frame are considered to be negligible small. In this analysis the properties of the air are allowed to change depending on the static temperature. The fuel to air ratio is expected to be very small. Due to this fact, the properties before and after the detonation are estimated assuming that the contribution of the burned fuel to Cp, γ and R is negligible and that the fluid before and after the detonation is only air.

$$Cp = Cp_{air}(T) \qquad R = 287\,\frac{J}{kg\ K} \qquad \gamma = \frac{Cp_{air}(T)}{Cp_{air}(T) - R}$$

This problem has been solved using the 1-D form of the equations of continuity, momentum and energy. These equations expressed in terms of the stagnation properties of the flow and the Mach number can be written as:

Continuity equation
$$\left(\frac{p_{t1}A_1}{\sqrt{T_{t1}}}\right)\sqrt{\frac{\gamma_1}{R}}\,D_1 = \left(\frac{p_{t2}A_2}{\sqrt{T_{t2}}}\right)\sqrt{\frac{\gamma_2}{R}}\,D_2$$

Momentum equation
$$p_{t1}A_1 G_1 + F_x = p_{t2}A_2 G_2$$

Conservation of energy
$$f\Delta HV = Cp_2 T_{t2} - Cp_1 T_{t1}$$

Where D, G and N are functions of M and γ

$$D(M,\gamma) = \frac{M}{\left(1 + \dfrac{\gamma - 1}{2}M^2\right)^{\frac{\gamma+1}{2(\gamma-1)}}}$$

$$G(M,\gamma) = \frac{1 + \gamma M^2}{\left(1 + \dfrac{\gamma - 1}{2}M^2\right)^{\frac{\gamma}{\gamma-1}}}$$

$$N(M,\gamma) = \frac{D(M,\gamma)}{G(M,\gamma)} = \frac{M\left(1 + \dfrac{\gamma - 1}{2}M^2\right)^{\frac{1}{2}}}{(1 + \gamma M^2)}$$

Shock wave

Shock waves are adiabatic by definition, so the stagnation temperature before and after the shock are equal. In addition, the shock does not add any external force into the flow. Dividing the continuity by the momentum equation the following relation arises

$$\sqrt{\gamma_1} N(M_1, \gamma_1) = \sqrt{\gamma_2} N(M_2, \gamma_2)$$

Heat addition region

As in the shock wave during the heat addition there are not external forces acting on the flow but, in this region, the stagnation temperature and pressure change. Dividing continuity by momentum and simplifying the energy equation the following equations are obtained:

$$\sqrt{\frac{\gamma_2}{T_{t2}}} N(M_2, \gamma_2) = \sqrt{\frac{\gamma_1}{T_{t1}}} N(M_1, \gamma_1) = \sqrt{\frac{\gamma_3}{T_{t3}}} N(M_3, \gamma_3)$$

$$f\Delta HV = Cp_3 T_{t3} - Cp_2 T_{t2} = Cp_3 T_{t3} - Cp_1 T_{t1}$$

Imposing the Chapman-Jouguet condition of choked flow after the detonation and solving this system of equations for M_1 it is possible to obtain the Mach number of the detonation wave $(M_1 = M_{CJ})$

$$\sqrt{\gamma_1 \frac{\frac{Cp_1}{Cp_3} T_{t1} + \frac{f\Delta HV}{Cp_3}}{\gamma_3 \quad T_{t1}}} N(M_1, \gamma_1) - N(M_3 = 1, \gamma_3) = 0 \quad where \ T_{t1} = T_1 \left(1 + \frac{\gamma_1 - 1}{2} M_1^2\right)$$

Once the Mach number of the detonation is known it is possible to determine all the other properties of the detonation.

The temperature after the detonation $(T_3 \ or \ T_{max})$ is obtained from the energy equation.

$$T_3 = T_{max} = \frac{f\Delta HV + Cp_1 T_{t1}}{Cp_3 \left(\frac{\gamma_3 + 1}{2}\right)}$$

The pressure ratio of the detonation is calculated using the following relations:

$$\frac{p_{t1}}{\sqrt{T_{t1}}} \sqrt{\gamma_1} D(M_1, \gamma_1) = \frac{p_{t3}}{\sqrt{T_{t3}}} \sqrt{\gamma_1} D(M_3 = 1, \gamma_3) \rightarrow \frac{p_{t3}}{p_{t1}} = \sqrt{\frac{T_{t3}}{T_{t1}} \frac{\gamma_1}{\gamma_3}} \frac{D(M_1, \gamma_1)}{D(M_3 = 1, \gamma_3)}$$

$$Pressure \ ratio = \frac{p_3}{p_1} = \frac{p_{t3}}{p_{t1}} \frac{\left(1 + \frac{\gamma_1 - 1}{2} M_1^2\right)^{\frac{\gamma_1}{\gamma_1 - 1}}}{\left(\frac{\gamma_3 + 1}{2}\right)^{\frac{\gamma_3}{\gamma_3 - 1}}}$$

In Table [] the results obtained from this code and CEA are compared for the case of burning hydrogen in air at stoichiometric fuel to air ratio $(T_1 = 750 \ K, \ p_1 = 2 \ atm)$

	Matlab code	CEA	Error [%]
Detonation Mach number [−]	2.868	3.029	5.32
Temperature after the detonation [K]	2474	3076	19.57
Detonation pressure ratio [−]	5.633	6.289	10.43

Table [4], detonation properties

Although there are discrepancies between both solutions the results are similar for most of the values. The main source of error comes from the fact that CEA solves the problem using chemical equilibrium and for the Matlab code we developed the flow is assumed to be composed only of air, neglecting the contribution of other species that will be present in the mixture.

13 Appendix F: Alternative RDE Analysis Model

This page intentionally left blank

An alternative model for the RDE combustor was considered. Although it was not used to solve the flow across the combustor in our final analysis, because it has not been used before by any research group, we think it is worth mentioning it.

The purpose of this method is to simplify the analysis of the RDE by looking at it from the reference frame of the detonation instead of looking at it from a fixed reference frame. By doing so the problem stops being a time dependent problem and an analytical solution can be found. However, some of the assumptions made in order to simplify the problem have not been proven to be correct. The main assumptions made are:

- The effect of the inertial forces can be neglected because they are small compared with other forces.
- The velocity in the azimuthal direction (v_θ) can be neglected in this analysis because it will not contribute to the thrust generation.
- Isentropic flow after the detonation.

In the reference frame of the detonation, all the physical properties of the flow (i.e. pressure, density, temperature,...) depend on the angular position in the combustor (θ) but not in time. The problem becomes steady. The change of reference frame has been made by means of the velocity of the detonation v_{CJ}

$$v_{CJ} = R_m \frac{d\theta}{dt} \quad where \ R_m = \frac{1}{2}(R_{out} + R_{in})$$

Integrating this equation and imposing the boundary condition that at $t = 0, \ \theta = 0$ the following relation between t and θ is obtained.

$$t = \frac{R_m}{v_{CJ}}\theta \rightarrow t_c = \frac{2\pi R_m}{v_{CJ}}$$

From experimental measurement it is known that the pressure decays exponentially with time.

$$p_c(t) = p_{min}PR_{CJ} \exp(-\lambda t) \quad where \ \lambda = \frac{\ln(PR_{CJ})}{tc}$$

Converting this equation into a function dependent on θ the following equation is obtained:

$$p_c(\theta) = p_{min}PR_{CJ} \exp\left(-\ln(PR_{CJ})\frac{\theta}{2\pi}\right) \quad where \ \theta \sim rad \quad \left| \begin{array}{l} p_c(\theta = 0) = p_{min}PR_{CJ} = p_{max} \\ \\ p_c(\theta = 2\pi \ rad) = p_{min} \end{array} \right.$$

Recalling the assumption of isentropic flow after the detonation the temperature evolution can be modeled as:

$$\frac{T_c(\theta)}{T_{max}} = \left(\frac{p_c(\theta)}{p_{min}PR_{CJ}}\right)^{\frac{\gamma-1}{\gamma}} \rightarrow T_c(\theta) = T_{max}\left(\frac{p_c(\theta)}{p_{min}PR_{CJ}}\right)^{\frac{\gamma-1}{\gamma}}$$

The mass flow at the exit of the combustor must be the airflow $(\dot{m}_0)$ plus the fuel mass $(\dot{m}_f)$. Applying mass continuity to a control volume that encloses the combustor volume the following relation arises.

$$\dot{m} = \dot{m}_0 + \dot{m}_f = \rho_c(\theta)u_c(\theta)A_{combustor} = \int_{R_{in}}^{R_{out}} \int_0^{2\pi} \rho_c(\theta)u_c(\theta)rdrd\theta$$

This equation cannot be solved because the shape of $u_c(\theta)$ is not known a priori. In order to obtain a solution the average value of $u_c(\theta)$ is used, $\bar{u}_c$ is an average value of $u_c(\theta)$.

Solving the equation for $\bar{u}_c$ the following analytical solution is obtained.

$$\bar{u}_c = \frac{\dot{m}}{\frac{1}{2}(R_{out}^2 - R_{in}^2)\,C} \quad where \ C = \frac{p_{max}}{RT_{max}}\frac{2\pi\gamma}{\ln(PR_{CJ})}\left[\exp\left(\frac{ln(PR_{CJ})}{\gamma}\right) - 1\right]$$

The stagnation properties can be calculated using $\bar{u}_c$ and assuming that v_θ is zero. Once these values are obtained the problem is closed and all the flow properties are known.

$$M_c(\theta) = \frac{\bar{u}_c}{\sqrt{\gamma R T(\theta)}}$$

$$T_{tc}(\theta) = T_c(\theta) + \frac{\bar{u}_c^2}{2Cp}$$

$$p_{tc}(\theta)$$
$$= p_c(\theta)\left(1 + \frac{\gamma - 1}{2} M_c^2(\theta)\right)^{\frac{\gamma - 1}{\gamma}}$$